Available online at www.sciencedirect.com
SCIENCE DIRECT®
Sensors and Actuators A 105 (2003) 137–149
SENSORS AND ACTUATORS A PHYSICAL
www.elsevier.com/locate/sna

Heat transfer in a MEMS for microfluidics

Nicolae Damean [a,*], Paul P.L. Regtien [a], Miko Elwenspoek [b]

[a] *Laboratory for Measurement and Instrumentation, Department of Electrical Engineering, University of Twente, P.O. Box 217, 7500 AE Enschede, The Netherlands*
[b] *Laboratory for Transducers Science and Technology, Department of Electrical Engineering, University of Twente, P.O. Box 217, 7500 AE Enschede, The Netherlands*

Received 19 July 2002; received in revised form 17 February 2003; accepted 12 March 2003

Abstract

Paper presents an 1D model for the heat transfer in a limited but significant region of an actuator–sensor structure for the determination of fluid and flow characteristics. As an essential step for the design of this structure, the usefulness of the model in the framework of the structure's functionality is underlined. In the first part of the work, the main heat transfer mechanisms are detailed by qualitative and quantitative evaluations. The 1D model is derived from the heat rate balance of the region we are interested in. In the second part of the work, we compare the data obtained by simulating the 1D model with the experimental data. Also, some full 3D simulations of the fluid flow and heat transfer are made using a commercial software package. Part of these numerical results are compared with the corresponding experimental data. The modeling errors are discussed for both sets of comparisons. Finally, we comment the merits of the 1D model versus the 3D approach. The results obtained herein might be directly used for various thermally based actuators and sensors for flow control and measurement both in micro and macro world.

Keywords: Actuator; Fluid; Heat; MEMS; Sensor

1. Introduction

The first flow sensor based on silicon technology was presented in 1974 by van Putten and Middelhoek [1], the fluid streaming around the sensor. After that, various thermal based sensors for flow measurement have been presented. In the 1990s, the development tends towards the fabrication of complex micro fluidic systems (micro flow sensors, pumps and valves in a system). Therefore, there is a need for a flow sensor that can measure very small flow rates. The result of this challenge is a new class of micromachined flow sensors which have an integrated micro duct. In this type of micromachined flow sensor, the fluid streams inside the sensor. The first sensor of this type was presented by Petersen in 1985 [2].

Flow sensors, like many others within the micro-electro-mechanical-system (MEMS) category display permanent evolution, from dedicated sensors (for a particular characteristic) to complex structures (designed for the evaluation of many characteristics of the fluid and its flow). This aspect is discussed in [3], where the authors developed a new measurement concept. Its core is an actuator–sensor structure (briefly structure). The concept is illustrated with a structure designed for the evaluation of fluid and flow characteristics. The study of the heat transfer in this structure is considered herein.

In this paper, the geometry and functionality of the structure are described firstly. We comment on its design steps and on the necessity of developing a local 1D model for the heat transfer in the structure. We detail the heat transfer mechanisms implied in the structure's functionality. They are evaluated for the practical ranges in which our structure is designed. The thermal balance of the region defining the structure's functionality is detailed, from which the 1D model is developed. Some comparisons between the experimental data when various gases are used (e.g. carbon dioxide, nitrogen, helium) and the modeling results are included to validate the 1D model.

Also, a full 3D simulation of the fluid flow and heat transfer is discussed. Its results are compared with the results offered by the 1D model for the region where this model is

* Corresponding author. Present address: Department of Chemistry and Chemical Biology, Harvard University, Mail Box #47, 12 Oxford Street, Cambridge, MA 02138, USA. Tel.: +1-617-4959436; fax: +1-617-4952500.
E-mail address: ndamean@gmwgroup.harvard.edu (N. Damean).
URL: http://www.people.fas.harvard.edu/~ndamean/.

0924-4247/03/$ – see front matter © 2003 Elsevier Science B.V. All rights reserved.
doi:10.1016/S0924-4247(03)00100-6

Nomenclature

a, b	dimensionless constants
A	cross-sectional area (m^2)
Bi	Biot number
c_p	constant pressure specific heat of the fluid (J kg K)
C, c	dimensionless constants
dz	differential element of the resistive line (m)
D	hydraulic diameter of the resistive line (m)
g	gravitational acceleration ($m\,s^{-2}$)
Gr	Grashof number
h	convection heat transfer coefficient ($W\,m^{-2}\,K^{-1}$)
H	depth (high) of the structure (m)
I	intensity of the direct electric current (A)
J	current density of the direct electric current ($A\,m^{-2}$)
k	thermal conductivity ($W\,m^{-1}\,K^{-1}$)
Kn	Knudsen number
L	width of the structure (length of the resistive line) (m)
N	number of resistors
Nu	Nusselt number
Pr	Prandtl number
R	electrical resistance (Ω)
Re	Reynolds number
$q_{conv}(z)$	convective heat rate for the differential element dz of the resistive line (W)
$q_{fluid}(z)$	conductive heat rate through the fluid to the silicon substrate for the differential element dz of the resistive line (W)
$q_{Joule}(z)$	Joule heat rate generated by the differential element dz of the resistive line (W)
$q_{rad}(z)$	radiative heat rate for the differential element dz of the resistive line (W)
$q_{solid}(z)$	conductive heat rate through the differential element dz of the resistive line to the silicon substrate (W)
$\dot{q}$	volumetric heat rate ($W\,m^{-3}$)
s	Seebeck coefficient ($V\,K^{-1}$)
T_a	ambient temperature (K)
$T_e(z)$	temperature of the resistive line in the point z (K)
T_r	recovery temperature (K)
$\Delta T(z)$	temperature difference $T_e(z) - T_a$ in the point z of the resistive line (K)
u	velocity component in the x-direction ($m\,s^{-1}$)
V_{av}	cross-sectional averaged velocity of the u-component of the velocity vector ($m\,s^{-1}$)
w	width of the resistive line (m)
x, y, z	Cartesian coordinates (m)

Greek letters

α	temperature coefficient of resistance of the resistive line (K^{-1})
β	volumetric coefficient of thermal expansion of the fluid (K^{-1})
δ, γ	dimensionless constants
ν	kinematic viscosity of the fluid ($m^2\,s^{-1}$)
ρ	electrical resistivity (Ω m)
θ	characteristic angle of the hexagonal duct (°)

Subscripts

e	associated with the equivalent material
f	associated with a fluid
i	integer

valid, but with the experimental data, too. Therefore, the 1D model validation is based on the experimental data and also on the 3D simulation.

Conclusions and remarks for the practical usage of this 1D model for the design of our actuator–sensor structure are included at the end. Also, we underline the importance of this model for the design purposes of various thermally based actuators and sensors for flow control and measurement both in micro and macro world. The usage of this model is restricted to the situation where the fully developed laminar flow of the incompressible and Newtonian fluids is concerned in connection with small temperature differences.

2. Description of the structure

A sketch of the structure we are designing is shown in Fig. 1. Its frame is made from two ⟨1 0 0⟩ Si wafers bonded together, both containing an etched groove. The structure looks like a hexagonal duct defined by the orientation of the silicon crystal planes with $\theta = 54.74^\circ$.

One electrical resistive line is placed across the duct in the region of the fully developed laminar flow. It consists of N resistors made of Pt film deposited on a Si_3N_4 carrier bridge placed along the z-axis over the width of the duct.

Sample used for experiments has the following dimensions: length along the x-axis is 40 mm, width along the z-axis is $L = 1$ mm, depth along the y-axis is $H = 502.2$ μm and $N = 25$. For assuring a fully developed flow for a large range of the fluid types and velocities, the resistive line is placed at 30 mm from the entrance. Main dimensions of the structure cross-section driven in the middle of the resistive line are shown in Fig. 2. Actually, the entrance and the exit are practically built as two holes through the top wafer.

The fabrication process of this structure and the experimental work are described elsewhere [4,5].

The voltages across each resistor are measured. The computational block controls the resistors to operate as tempera-

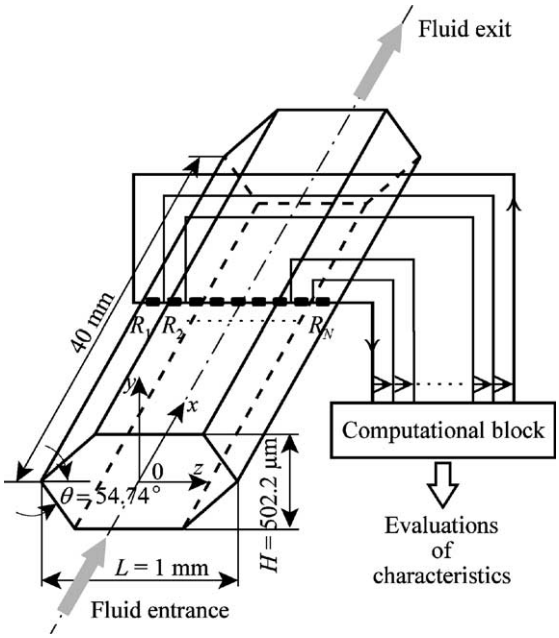

Fig. 1. Sketch of the structure.

ture actuators and as temperature sensors. This block evaluates the characteristics we are looking for (like velocity (u), kinematic viscosity (ν) and thermal conductivity (k) of the fluid) using the data provided by the resistors and a priori information as: the model of the structure, the activation of the actuators, the evaluations fulfilled by the sensors and the initial information about the fluid and its flow.

Carbon dioxide, helium and nitrogen have been used as the measurement fluids for the experiments. We consider their Prandtl number Pr as 0.75, 0.68 and 0.71, respectively.

The direct current I passing the resistive line is smaller or equal than 2.5 mA for nitrogen, but smaller or equal than 5 mA for carbon dioxide and helium.

For carbon dioxide, helium and nitrogen, the Reynolds number Re takes a value in the range 31–155, 11–59 and 27–136, respectively, because the averaged velocity V_{av} is in the range 0.396–1.98, 2.176–10.88 and 0.66–3.3 m s^{-1}, respectively, in the experimental work described in [5].

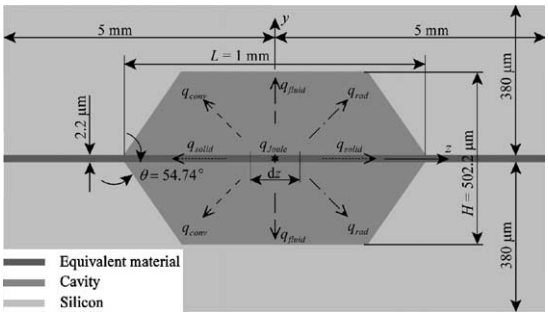

Fig. 2. Heat transfer mechanisms and main dimensions of the structure cross-section.

Therefore, we consider a laminar flow of an incompressible and Newtonian fluid through this duct. Actually, this is the usual regime for the micro fluidic devices [6].

The ambient temperature T_a is 300 K throughout this paper. We consider the ambient temperature T_a equals the fluid free stream temperature (temperature of the fluid far away from the resistive line vicinity). Temperature differences less than 40 K relatively to the ambient temperature have been experienced inside the structure.

3. Design steps of the structure

The design of the structure depends on two physical phenomena: the fluid flow through the structure and the heat transfer in the fluid and in the solid part. They should be considered independently from each other in the case of small temperature differences.

Two consequences of the small temperature differences have immediate implications upon the design steps.

One consequence is that all physical properties are weakly temperature dependent. Actually, we consider their values at 320 K because the structure temperature (K) might vary in the range 300–340 K. For this range, the physical properties of the materials used in the structure's fabrication as well as the physical properties of a large number of fluids might modify with maximum ±4% if we consider 320 K as the reference temperature [7,8].

Another consequence of the small temperature differences is that the measurement procedure does not modify the characteristics of the fluid and of the flow.

The design steps of the structure are formally described in [3], the second consequence mentioned above being the main applicability condition for this formalization.

Firstly, we analyzed the fluid flow through the structure. An analytical formula for the velocity field u_i corresponding to each resistor R_i is detailed in [9]. Then, the Poiseuille number for hexagonal ducts is discussed in [10]. Finally, we use these results for the heat transfer analysis. This task is addressed herein.

Practically, the final target of the design is to describe simply the dependencies of the characteristics mentioned above on R_i as these entities are directly measured. Because these dependencies are implied by the heat transfer in the fluid and in the solid part, a simple approach should be developed for the heat transfer analysis in the resistive line.

We develop an 1D model for the heat transfer in the resistive line. This model takes into consideration the main heat transfer mechanisms in the structure correlated with the fluid flow, but gives only local information we are looking for, namely the dependencies of the characteristics mentioned above on R_i.

Our approach contrasts with the classical approaches based on 2D or 3D models in the heat transfer and fluid flow domains [11]. Some essential advantages for using this

1D model are: short computation time during simulation and its suitability for the optimization implied by the design steps as well as for the identification problems raised by the determination of the characteristics we are looking for. Its main disadvantage might be that it has a limited usage in respect of the modeling errors. This aspect should be verified a priori by experiments as well as 3D simulations. Both verifications are included herein.

We mention that Knudsen number *Kn* is still low enough for the continuum flow model to be valid. Velocity-slip and temperature-jump boundary conditions are not necessary when solving the momentum and energy equations. This point has been already discussed in [9].

4. Developing the 1D model of the resistive line

Consideration is given to the heat transfer mechanisms which might be implied in the structure's functionality, namely: heat generation by Joule effect, conduction in the fluid and in the solid part, (free and forced) convection and radiation in the fluid.

We evaluate the contribution of each of these mechanisms and finally we ensemble them in an 1D model describing the temperature difference of the resistive line.

4.1. General description of the heat transfer mechanisms into the structure

Full Navier–Stokes equation solvers have been used for computing the fluid flow in micro ducts [12]. Because of its small depth, the velocity component and pressure difference in the lateral direction are negligibly small in comparison with those in the longitudinal direction of a duct [13].

In Fig. 2, we display the heat transfer mechanisms in the structure. The structure is operating in the steady-state of the direct current.

The temperature distribution in the resistive line is determined from the heat rate balance for a generic differential element dz. Its various components constitute sources and sinks [7].

The resistive line is provided with electrical power to generate Joule heat, whose rate is q_{Joule}. This denotes source while the loss mechanisms denote sinks.

The component q_{solid} describes the rate of the conductive heat loss through the resistive line to the silicon substrate. In contrast to the situations normally encountered in ICs, q_{solid} in this structure (as in other similar micromachined structures) is dramatically lowered by virtue of thermal isolation. With the removal of the silicon substrate, a huge conductive component directly below and above the resistive line is eliminated resulting in low power (a few mW) structure operation as well as thermal time constant (a few ms). The maximum power operation is about 2.5 mW in our case. Consequently, the other heat sink mechanisms gain significance.

For example, even in the absence of fluid motion, there is a non-negligible heat rate loss component q_{fluid} to the fluid above and below the resistive line. Part of q_{fluid} may return to a cooler part of the resistive line. This is significant when the temperature of the resistive line is highly nonuniform, as we expect that it happens in our situation.

The component q_{conv} denotes heat transfer rate by forced and free convection. Forced convection occurs in the presence of fluid flow stream, but free convection occurs when fluid motion is caused by internal buoyancy forces stemming from temperature differences within the fluid, which give rise to density variations. Free convection may be neglected in many micro structures operating at not too large temperatures. We are going to prove that this is the case for our structure. Here we mention only that the buoyancy term which depends on the magnitude of the Rayleigh or Grashof number is neglected in the momentum equation since these numbers are proportional to the third power of the characteristic length for a convection problem. Therefore, the value of the Rayleigh or Grashof number is very small for micro duct flow [13].

The component q_{rad} denotes the rate of the radiative heat loss component. It is relatively small at standard environmental temperature and pressure, and for not too large resistive line temperature [7]. We are allowed to neglect this component as we show later.

Therefore, the heat rate balance for the differential element dz is:

$$q_{\text{Joule}} = q_{\text{solid}} + q_{\text{fluid}} + q_{\text{conv}} + q_{\text{rad}} \quad (1)$$

where a priori each of the terms is *z*-dependent.

For making the theoretical development easier, we consider the resistive line being manufactured of a single material denoted as equivalent material as it is presented in Fig. 2. The geometry and thermal conductivity of the equivalent material are calculated considering that the thermal resistances of the both components of the resistive line are connected in a parallel circuit. For the sake of clearness, when confusions are possible, we use the subscript 'e' to show that we speak about the equivalent material.

Also, in a similar manner with thermal conductivity, we may calculate the electrical resistivity of the equivalent material. However, we notice that the electrical resistivity of Pt is much smaller than the electrical resistivity of Si_3N_4, therefore we consider the electrical resistivity of Pt for the equivalent material.

4.2. Design requirements for the resistive line

There are two main requirements for the design of the resistive line. They concern the power generation and electromigration [14].

The superior limit of the power is defined by the requirement to get relatively small temperature differences (not more than 40 K) as we discussed before. During the experiments, we noticed that this requirement is met if the val-

ues of the direct current I is in the ranges we displayed previously.

Besides the power requirement, it is essential to make sure that the current density of the resistive line does not exceed the electromigration limit of Pt ($\approx 10^{10}$ A m^{-2}). The current density is calculated by $J = I/A_{\mathrm{Pt}}$, where A_{Pt} is the cross-section area of the Pt film from the composition of the resistance line. Using this formula, we get for the direct current I a value of about 10 mA.

The temperature coefficient of resistance of the resistive line is given in [4,14], with values $\alpha = 2 \times 10^{-3}$ and 1.8×10^{-3} K^{-1}, respectively.

4.3. Simplifications from 3D to 1D model

The simplifications detailed herein are determined by the necessity in getting an 1D model. It has to be acceptable both from a physical point of view and for design purposes.

The physical behavior of the structure takes place in the 3D space. The fluid flow behavior is actually reflected in the thermal behavior of the resistive line.

In view of getting a simple model for describing the thermal behavior of the resistive line, we make two statements that are justified in the following.

We neglect the effects of the thermal dissipation of mechanical energy into thermal energy through viscous friction. These effects are significant in connection with high speed aerodynamics in which the fluid velocities are sufficiently high. Such effects are present in both compressible and incompressible flow. An example of incompressible flow where the effect of viscous dissipation might be encountered is in the use of highly viscous oils in lubrication applications [15]. In our case, we evaluate the dissipative effects by calculating the difference between the recovery temperature T_{r} and the free stream temperature T_{a} as [15]:

$$T_{\mathrm{r}} - T_{\mathrm{a}} = Pr^{0.5} \frac{V_{\mathrm{av}}^2}{2c_p} \tag{2}$$

Applying Eq. (2) for the gases we used in the velocity ranges mentioned above, the values we get are smaller than 0.01 K. Therefore, this omission is justified.

The thermal behavior of the resistive line might be described using an 1D model along the z-axis. To check this hypothesis, we estimate the Biot number Bi for the x- and y-directions of the resistive line using the general formulae [16,17]:

$$Bi = \frac{h\ell}{k_{\mathrm{e}}} \tag{3}$$

$$Nu = \frac{h\ell}{k_{\mathrm{f}}} \tag{4}$$

where ℓ is the characteristic length of the resistive line along the x- and y-directions, respectively, and h the convection heat transfer coefficient for the same directions. To estimate h for the both directions respectively, we calculate the averaged Nusselt number Nu using two classical formulae that might be roughly valid in our situation, namely

$$Nu_w = 0.644\, Re_w^{0.5}\, Pr^{0.33} \tag{5}$$

$$Re_w = \frac{V_{\mathrm{av}} w}{\nu} \tag{6}$$

for the forced convection along surfaces, and

$$Nu_D = 0.75\, Re_D^{0.4}\, Pr^{0.37} \tag{7}$$

$$Re_D = \frac{V_{\mathrm{av}} D}{\nu} \tag{8}$$

in the case of forced convection for external flow normal to tubes. Using Eqs. (3)–(8), we get values for Bi that are much smaller than unity. Therefore, we might consider that temperature of the resistive line does not vary essentially along the x- and y-directions, the only variation is along the z-direction. This remark entitles us to look for an 1D model of the thermal behavior of the resistive line instead of a 3D one.

Each term of the heat rate balance described by Eq. (1) is addressed next.

4.4. Joule heat generation

We use the same resistive line both for actuating and also for sensing. The actuating function is performed by heating up simultaneously all the resistors that constitute the resistive line. The sensing function is performed by each resistor apart.

We assume that the structure is not subject to magnetic or mechanical fields; this permits a scalar description for both electrical and thermal transport coefficients. We further assume that there is no interaction of carriers with optical fields.

Under non-isothermal conditions, the presence of a temperature gradient causes additional coupling between electrical and heat transport in semiconductors and metals. The coupling gives rise to a number of electrothermal effects, notably, the Seebeck, Peltier, and Thomson effects, whose magnitude depends on the material type as well as electrical and thermal operating conditions.

Because the structure involves thin film conductors, several assumptions can be invoked to simplify constitutive (or transport) equations. These are reviewed in [7]. In the steady-state regime for the resistive line, we get the volumetric heat generation:

$$\dot{q} = J^2 \rho_{\mathrm{e}}(T_{\mathrm{e}}) + T_{\mathrm{e}} \cdot J \cdot \nabla s(T_{\mathrm{e}}) \tag{9}$$

where $\rho_{\mathrm{e}}(T_{\mathrm{e}})$ and $s(T_{\mathrm{e}})$ denote the temperature-dependent electrical resistivity and Seebeck coefficient, respectively.

Seebeck coefficient plays a crucial role as it determines electrical transport in the presence of a temperature difference and heat transport in the presence of a potential difference.

The first term of the right-hand side (r.h.s.) of Eq. (9) corresponds to the well-known Joule heating (that is irreversible phenomena) and the second term accounts for both Peltier and Thomson heating (that are reversible phenomena) [15]. Peltier heating describes the heat that goes along with an electric current at an interface of materials with different Seebeck coefficients. Thomson heating describes the heat that accompanies the flow of an electric current in the presence of a temperature difference, and is significant only when the Seebeck coefficient is strongly temperature-dependent [13]. Actually, the second term of the r.h.s. of Eq. (9) corresponds to the Seebeck effect resulted as a combination of the Peltier and Thomson effects. Estimating both terms of the r.h.s of Eq. (9), we notice that the ratio between the first and the second term is in the order of 10^3. Therefore, we neglect both Peltier and Thomson heat.

We deliberately skip the electrical transport equation that should join the heat transport Eq. (9) in describing the electrothermal behavior of the resistive line. The reason is that we consider the electrical potential being constant for the differential solid element dz. This hypothesis is supported by the small temperature differences along and across the differential element and also by the operation of the resistive line under I = constant.

Finally from Eq. (9) we get the Joule heat rate generated by the differential element of the resistive line:

$$q_{\text{Joule}} = \frac{I^2 \rho_e(T_e)}{A_e}\,\mathrm{d}z \tag{10}$$

where

$$\rho_e(T_e) = \rho_e(T_a)(1 + \alpha\,\Delta T(z)) \tag{11}$$

and

$$\Delta T(z) = T_e(z) - T_a \tag{12}$$

because of the small temperature differences in each point of the resistive line.

4.5. Conductive heat transfer

Our target is to get valid information in view of the determination of fluid and flow characteristics. Therefore, we intend to get a reliable model under zero and non-zero flow as well. This necessity is particularly stressed by the particular behavior of the structures like ours where a significant percentage of the input power is transferred to the surroundings [7].

Using the Fourier law of heat conduction [17] for the differential element, we get the conduction heat transfer rate:

$$q_{\text{solid}} = -A_e k_e \frac{\mathrm{d}^2 T_e}{\mathrm{d}z^2}\,\mathrm{d}z \tag{13}$$

To evaluate q_{fluid}, we have to solve the following 3D heat conduction equation for the stagnant fluid:

$$\frac{\partial^2 T_f}{\partial x^2} + \frac{\partial^2 T_f}{\partial y^2} + \frac{\partial^2 T_f}{\partial z^2} = 0 \tag{14}$$

Boundary conditions of Eq. (14) are of the Dirichlet type, including the temperature T_a as well as the temperature T_e of the differential solid element we consider.

Because of the analytical difficulties in solving Eq. (14), we use a simple procedure based on the non-dimensional shape factor $G(z)$ [18,19]:

$$G(z) = \begin{cases} \delta\left(\dfrac{z}{L}\right)^{\gamma} & \text{if } z \in \left[0, \dfrac{L}{2}\right] \\ \delta\left(1 - \dfrac{z}{L}\right)^{\gamma} & \text{if } z \in \left[\dfrac{L}{2}, L\right] \end{cases} \tag{15}$$

where δ and γ are positive constants that are determined from the experimental data using a standard least-square procedure. Therefore, we approximate q_{fluid} like:

$$q_{\text{fluid}} = G(z) k_f\,\Delta T(z)\,\mathrm{d}z \tag{16}$$

For getting confidence in this approximative approach, the authors applied it for a similar situation that has been solved fully analytically.

We approximate our hexagonal structure with a rectangular one. An analytical 3D model describing the heat transfer in the resistive line placed in the rectangular duct is given in [20]. We apply our approximative approach, getting the values of δ and γ for the rectangular duct. Then, for each of N resistors we calculate the relative error between the temperatures calculated by this approach and the temperatures derived by the analytical approach described in [20]. The maximum relative error is 0.87% for the gases we used in the current and velocity ranges we are interested in.

Next, we consider the case of the hexagonal structure we are designing. The values of and are obtained from the experimental data given in [4,5]. We get $\delta = 232.43$ and $\gamma = 1.8$. The maximum absolute relative error between the temperatures calculated with the model described by Eqs. (1), (10)–(13), (15), (16) and the experimental data is 1.21%.

We stress that the $G(z)$ mapping (defining the conductive transfer in the fluid) is dependent only on the geometry of the duct. Thus, $G(z)$ mapping derived here might be useful for another working conditions if the same structure dedicated for the fluid flow measurement is implied.

4.6. Convective heat transfer

4.6.1. Free convection heat transfer

We analyze the significance of the free convection over forced convection as well as over the conductive heat transfer in the fluid. This analysis is imposed by the necessity to get an acceptable 1D model for the heat transfer in the structure either in the situation of stagnant fluid and laminar flow.

Firstly, we estimate the lower bounds for the fluid velocity that assure pure forced convection. It states that the lower bound of significant forced convection for a horizontal plate

along the x-axis is given by the formula [21]:

$$\frac{Gr_x}{Re_x^{2.5}} \leq 9.5 \tag{17}$$

where

$$Gr_x = \frac{g\beta(T_e - T_a)x^3}{\nu^2} \tag{18}$$

$$Re_x = \frac{ux}{\nu} \tag{19}$$

In Eq. (18), the volumetric coefficient of thermal expansion β is considered like $2/(T_e+T_a)$, that is a reasonable approach as stated in [22], it is even valid only for a perfect gas.

We apply Eqs. (17)–(19) for each resistance by averaging along w, the width of the resistive line. For the three fluids, carbon dioxide, helium and nitrogen, we get the lower bounds of significant forced convection in terms of the averaged velocities: 1.29×10^{-2}, 2.2×10^{-2} and $1.47 \times 10^{-2}\,\mathrm{m\,s^{-1}}$, respectively. These values are more than 30 times lower than the inferior bound of the averaged velocity values of the corresponding fluids. We see also that excepting the vicinity of first and the last resistor which are not practically used for measurements, we face only situations where the forced convection heat transfer dominates the free convection heat transfer.

Secondly, we analyze the significance of the free convection over the conductive heat transfer in the fluid.

In [23] it is shown that for heated elements in close proximity to other objects, the effects of the free convection are suppressed. Namely, it is stated that for Grashof numbers under 2000, free convection is not important, and most of the heat transfer is through conduction. For the averaged Grashof numbers over the width of the resistive line we get the following values: 3.47×10^{-2}, 1.64×10^{-4}, and 9.75×10^{-3}, respectively. From this rough estimation, we conclude that the free convection heat transfer is insignificant in comparison with the conductive heat transfer in the fluid.

Following a more detailed approach, we calculate the ratio between the free convection heat transfer and conductive heat transfer using the results exposed in [21] for the free convection heat transfer corresponding to the horizontal plate and Eqs. (15) and (16) for the conductive heat transfer in the fluid. Averaging over the width of the resistive line, we get for this ratio a value having the shape $c/G(z)$, where the constant c takes the values 0.31, 0.1 and 0.23, respectively, for the three fluids we consider. An algebraic calculus shows this ratio is about 0.3 for the first and the last resistor and about 0.1 for the second and the second last resistor. Of course, this ratio is smaller for the other resistors.

Therefore, we are entitled to neglect the free convection heat transfer in comparison with the conductive heat transfer in the fluid.

4.6.2. Forced convection heat transfer

Besides the conductive heat transfer, the forced convection heat transfer plays an important role in the heat rate balance described by Eq. (1). The heat transfer from a hot sensing element immersed in a fluid increases with the flow rate.

Sensors employing the relation between the heat transfer and the flow are usually referred to as thermal anemometers. They have been widely used since the introduction of the hot-wire anemometer in the beginning of this century [24].

Heat is transferred by forced convection from both surfaces (upper and lower) of the resistive line.

When there is no flow, the temperature distribution of the differential element varies along z-axis only as we concluded earlier (based on Bi number estimation).

In the presence of a fluid flow, the heat transfer from the surface of the differential element (initially at uniform temperature) is not distributed uniformly, but is largest at the upstream side where the flow first encounters the hot surface. Because of this nonuniform cooling effect, a small temperature difference is induced over the resistive line. The uniformity increases with the flow velocity and is sensitive to the flow direction [25]. Nevertheless, the flow velocity is relatively small, so we consider that the temperature of the differential element is uniform also during cooling. This is supported by the small width of the resistive line.

Above a certain flow velocity in a duct, only a region of the flow near the resistive line is heated, and a thermal boundary layer is formed over the sensor. As the thickness of the velocity boundary layer (and therefore the amount of flow that is affected) decreases with the increasing velocity, the heat transfer increases less linearly in relation to the flow velocity [24].

In the case of a flow with uniform velocity, we calculate the forced convection heat transfer rate from the differential element as:

$$q_{conv} = 2w\,\mathrm{d}z\,h_w(T_e(z) - T_a) \tag{20}$$

where h_w is the local convection heat transfer coefficient at the ending edge of the differential element. This coefficient has to be determined next.

As noted in [16], pure forced convection heat transfer may be expected to be of the form.

$$Nu = f(Re, Pr) \tag{21}$$

when the effects of dissipation of mechanical energy through viscous friction are neglected.

The specialized literature presents some situations that become classical now for the pure forced convection heat transfer. Instances in which empirical methods are used, the resulting formulas are almost invariably presented in the form described by Eq. (21).

However, certain effects such as the temperature dependence of properties, the influences of the starting length, the effects of the confined flow on the boundary layer, etc., may necessitate the inclusion of additional parameters. More than that, the uncertainties in the many fluid properties involved,

experimental errors, geometrical deviations, surface roughness, etc., may cause considerable deviation between theory and experiment or scatter in the correlation of experimental data. As a result, such deviations or scatter of the order of magnitude of ±10% in predicted Nusselt numbers are not uncommon in forced convection [16].

A common procedure is to use Eq. (20), where the local convection heat transfer coefficient h_w is defined based on the local Nusselt number Nu_w as

$$Nu_w = \frac{h_w w}{k_f} \tag{22}$$

where Nu_w is detailed by Eq. (5) and the local Reynolds number Re_w is z-dependent being defined by Eq. (23)

$$Re_w(z) = \frac{u(z)w}{\nu} \tag{23}$$

because the convective heat transfer from a flat plate is concerned.

Eqs. (5), (6), (20), (22) and (23) state that if the fluid flow is laminar, the heat transfer scales as $Re_w^{0.5}$. It was proved many years ago that this holds for flat plates [26], and also for hot-wires [27].

In the field of micro structures, experimental support for the square root behavior is given in many works, e.g. [12,28]. At low flow rates, however, there is a significant deviation from the square root behavior. In addition, for different geometries, due to an interaction of a buoyant plume and the forced convection flow component, unsteady phenomena may occur at very low velocities [29].

Main reason of these drawbacks is that we tacitly consider that the boundary layer approximation holds for situations like ours (confined and low velocity fluid flow over a flat plate). Unfortunately, we notice rather straightforward that this is not true, since for very low velocities or very small narrow resistive lines, the boundary layer approximation does not hold [29].

A simple criterion for the boundary layer approximation's validity is $Re_w^{0.5} \gg 1$ [17,29]. For carbon dioxide, helium and nitrogen flowing in their velocity ranges, we get that $Re_w^{0.5}$ belongs to the ranges 2.17–4.85, 1.33–2.98 and 2.04–4.56, respectively. Therefore, the criterion for the boundary layer approximation's validity does not hold in our case.

Apparently, this inconvenience disappears when higher fluid velocities are considered. Unfortunately, on another hand, we cannot do anything about the small width of the resistive line, because the boundary layer approximation given by Eq. (5) does not hold in the immediate vicinity of the tip of the boundary layer region (as one property of the square function is that it has infinite slope in the origin) [17].

This feature is being stressed because it is rarely considered in the boundary layer works that appear in books and journals [7,30,31]. In conclusion, we should use the results concerning the boundary theory approximation in a careful manner by checking the applicability hypotheses first.

Taking into consideration, the complexity of the physics involved in such studies like ours, we adopt a simplified form for Nu_w, namely

$$Nu_w = C\, Re_w^a\, Pr^b \tag{24}$$

where the constants C, a and b are determined using a standard least-square procedure by comparison with the experimental data. This approach is derived from the well-known King's law [27].

In Section 5, we get $C = 0.339$, $a = 0.6$ and $b = 3.9$. The maximum absolute relative error between temperatures calculated with the model described by Eqs. (1), (10)–(13), (15), (16), (20), (22)–(24) and the experimental data is 5.86%, as shown in Section 5.

4.7. Radiation heat transfer

Another heat transfer mechanism that bears consideration is radiation. In a large majority of micro structures, the heat transfer by radiation is generally insignificant relative to the other components at standard (atmospheric) pressure.

To establish an upper bound for radiative heat transfer, a hypothetical configuration of the resistive line can be constructed. Assume the emissivity is 1, and that the element is surrounded by a conformal blackbody cavity at T_a temperature. This means that the resistive line radiates heat energy, but receives no energy back through radiation. For this worst-case situation, using Eqs. (10)–(12) and the Stefan–Boltzmann law, we get $q_{rad}/q_{Joule} = 5.5\%$, but the actual value is less. Radiative heat transfer will be neglected in all subsequent analysis.

At the end of Section 4, we include a remark concerning the heat transfer mechanisms. As Eq. (1) states, we consider the heat transfer rate by conduction in the fluid and heat transfer rate by (free and forced) convection as two distinctive quantities. In the case of stagnant flow, neglecting the free convection heat transfer, we notice that q_{conv} vanishes, but q_{fluid} plays a central role. For both stagnant flow and fluid flow, q_{fluid} depends on z, because of the structure's geometry. Also, q_{conv} depends on z because of the velocity field of the fully developed laminar flow in a hexagonal duct. As these two quantities depend on z following distinctive rules, we consider them in two distinctive terms.

This approach is different than classical approaches for external free convection flow concerning common immersion geometries (as plates, cylinders or spheres). In these situations, the heat transfer is described like $Nu = Nu_0 + f(Gr, Pr)$, where Nu_0 is a constant and f is a function depending on Grashof and Prandtl numbers [8]. The classical approaches are developed under the hypothesis that the common immersion geometries are isothermal.

5. Validation of the 1D model

From Eqs. (1), (10)–(13), (15), (16), (20), (22)–(24) we conclude that the temperature difference along the resistive

line is given by the linear second-order partial differential equation with variable coefficients:

$$\Delta T_{zz} = \frac{\Delta T}{A_e k_e}\left(\frac{I^2\rho_e\alpha}{A_e} - G(z)k_f - 2C\left(\frac{u(z)w}{\nu}\right)^a Pr^b k_f\right) + \frac{I^2\rho_e}{A_e^2 k_e} \quad (25)$$

where $G(z)$ is given by Eq. (15) and the parameters' values are $\delta = 232.43$, $\gamma = 1.8$, $C = 0.339$, $a = 0.6$ and $b = 3.9$.

Eq. (25) is associated with Dirichlet boundary conditions, in our case the temperature differences of both ends of the resistive line.

The procedure of getting the values of δ and γ is described in Section 4.5. We use these values for getting estimations for the parameters C, a and b from Eq. (25). This is briefly described next.

Firstly, we consider nitrogen as the tested fluid. We are looking for an estimation of the parameter a around 0.5, as Eq. (5) suggests, and also an estimation of the product CPr^b. These two estimations are obtained using the least-square methodology as the values producing the minimum deviation between the experimental data and the data obtained by simulating the 1D model described by Eq. (25). We denote $\{a, CPr^b\}\_N_2$ the pair of the estimations we obtain for nitrogen. In the same manner, we proceed for helium and carbon dioxide, and we get the estimations $\{a, CPr^b\}$_He and $\{a, CPr^b\}\_CO_2$, respectively. Analyzing these pairs, we notice that the estimations of the parameter a are very close to 0.6 for all three gases, so we consider $a = 0.6$ for these gases.

Secondly, we recalculate for each gas the estimation of the product CPr^a in the same manner we did it previously, but this time we set $a = 0.6$. We get three estimations of the product CPr^b, namely $CPr^b\_CO_2$, CPr^b_He and $CPr^b\_N_2$, for three gases, respectively. These estimations lead to three nonlinear equations having two unknowns, namely the parameters C and b. The unique solution of this system is approximated using the least-square methodology, so finally we get $C = 0.339$ and $b = 3.9$ for all the three gases.

In the following, the 1D model given by Eq. (25) is validated in two steps.

Firstly, we compare the predictions given by the 1D model with the experimental data, when the carbon dioxide, helium and nitrogen are used in velocity and electric direct current ranges we consider currently.

Secondly, we compare the previous two sets of data with the results offered by a full 3D simulation of the fluid flow and heat transfer.

5.1. Experimental verification

We include in Figs. 3–9 the comparisons between the predictions given by the 1D model described by Eq. (25) and the experimental data for three gases and various direct currents.

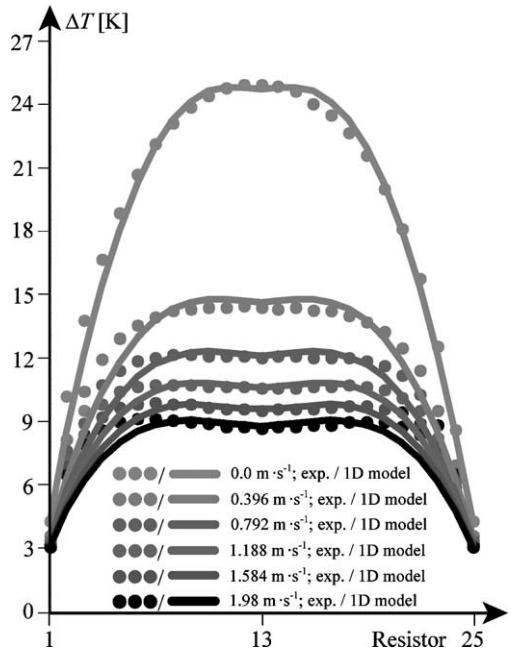

Fig. 3. Temperature difference of each resistor for a current of 2.5 mA and various velocities of CO_2.

The experimental work is carried out by Dr. John van Baar and is described elsewhere [4,5].

For each pair experimental curve/modeling curve, we calculate the modeling error as follows. Firstly, for each resistor we calculate the absolute value of the relative error between the modeling and experimental data result. Lastly, the modeling error is calculated by averaging over N.

We proceed in this manner for carbon dioxide, helium and nitrogen for each value of the velocity.

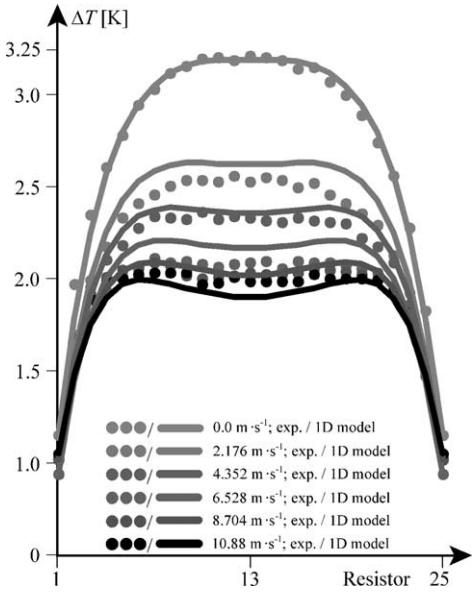

Fig. 4. Temperature difference of each resistor for a current of 2 mA and various velocities of He.

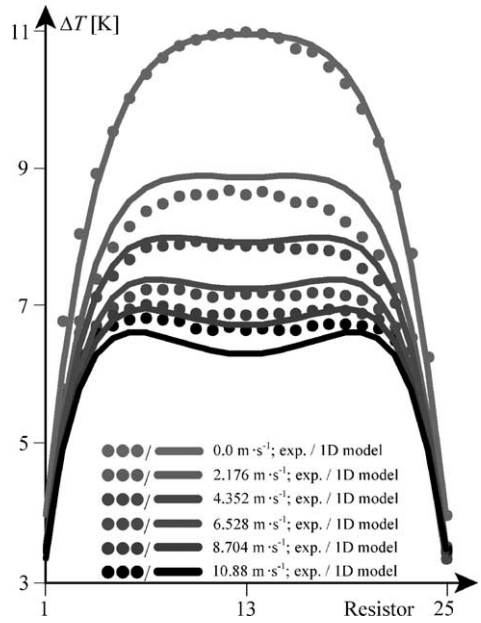

Fig. 5. Temperature difference of each resistor for a current of 3.5 mA and various velocities of He.

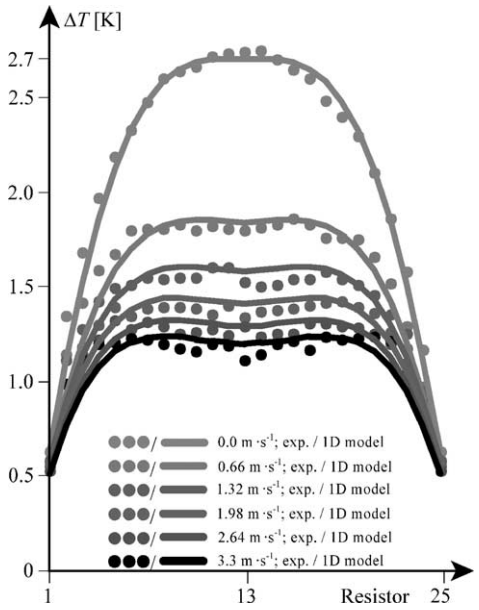

Fig. 7. Temperature difference of each resistor for a current of 1 mA and various velocities of N_2.

We find that the maximum value of the modeling error is 5.86% that is an acceptable error if we take into consideration many simplifications we made in the process of deriving the 1D model for a system whose behavior is 3D.

Inspecting Figs. 3–9, we notice that the biggest relative differences between the data given by the 1D model and the experimental data are localized at the extremities of the resistive line, near the wall. This behavior is expected because the influence of the wall is simplified very much both in the conductive and convective part of the 1D model.

Another source of error is formed by the uncertainties in the physical properties of the materials that are used in the structure's fabrication as well as in the physical properties of the fluid. Based on experiments and simulations, we estimate their influence on the temperature differences at 1%.

5.2. *Verification by 3D simulation*

We perform some full 3D simulations for the fluid flow and heat transfer in this structure.

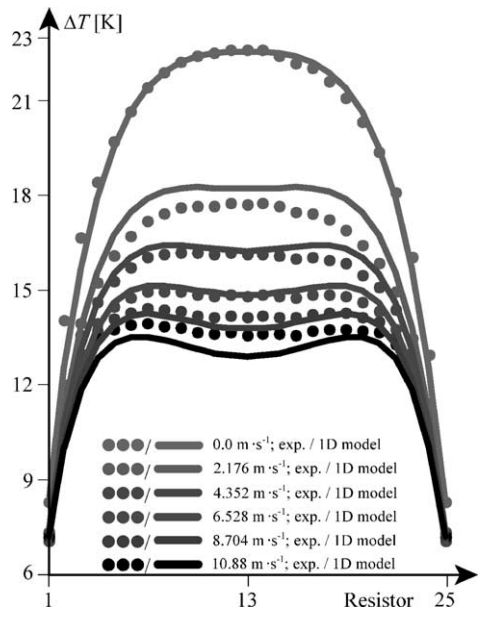

Fig. 6. Temperature difference of each resistor for a current of 5 mA and various velocities of He.

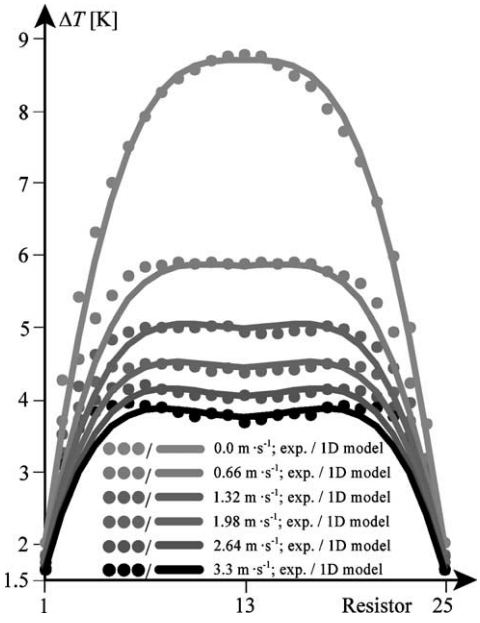

Fig. 8. Temperature difference of each resistor for a current of 1.75 mA and various velocities of N_2.

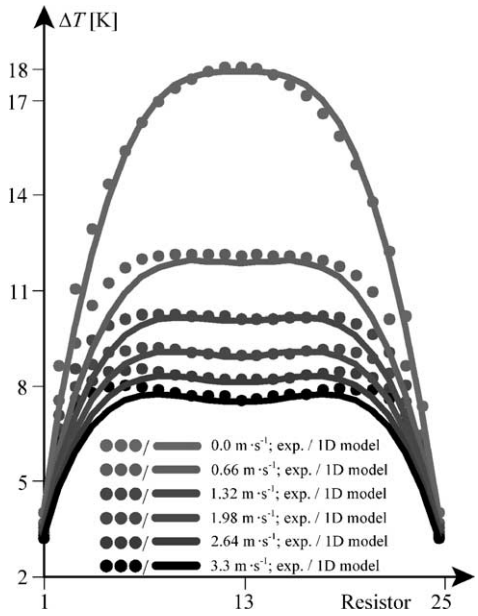

Fig. 9. Temperature difference of each resistor for a current of 2.5 mA and various velocities of N_2.

We have used the CFD-ACE+ software package based on the finite volume method [32].

Because the time consumption of these simulations is big in correlation with the hardware we used (PC—1 GHz) and the mesh we have built (163,270 nodes), we consider only the case when nitrogen is flowing with an averaged velocity of 3.3 m s^{-1} and the resistive line is loaded by a direct current of 2.5 mA.

Some results of these simulations are presented in Figs. 10–12. We represent the status of the fluid flow (respectively the *u*-velocity) and the temperature difference ΔT when the fluid is in rest and also when it is flowing.

The representations are made around the resistive line in the *x*–*y* plane of Fig. 1. Thus, only a range of 1 mm length of the duct is represented, but the length of the duct is 40 mm.

From these figures, we see that this vicinity determines the functionality of the structure.

Similar to Fig. 9, we present in Fig. 13 two sets of curves corresponding to the fluid in rest and to the fluid flowing with an averaged velocity of 3.3 m s^{-1}.

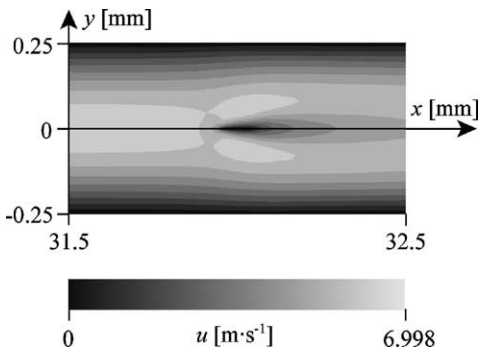

Fig. 10. The *u*-velocity when $V_{av} = 3.3\,m\,s^{-1}$ for N_2.

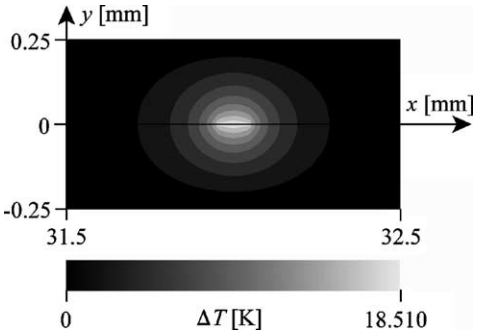

Fig. 11. ΔT when $V_{av} = 0\,m\,s^{-1}$ for N_2.

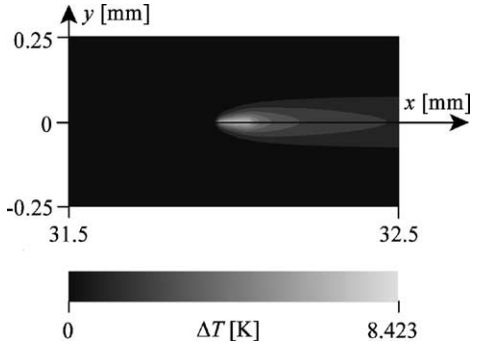

Fig. 12. ΔT when $V_{av} = 3.3\,m\,s^{-1}$ for N_2.

These curves show the temperature difference of each resistor of the resistive line.

Each set of curves consists of three curves corresponding to the experimental data, the 1D model we derive and the full 3D simulation we perform.

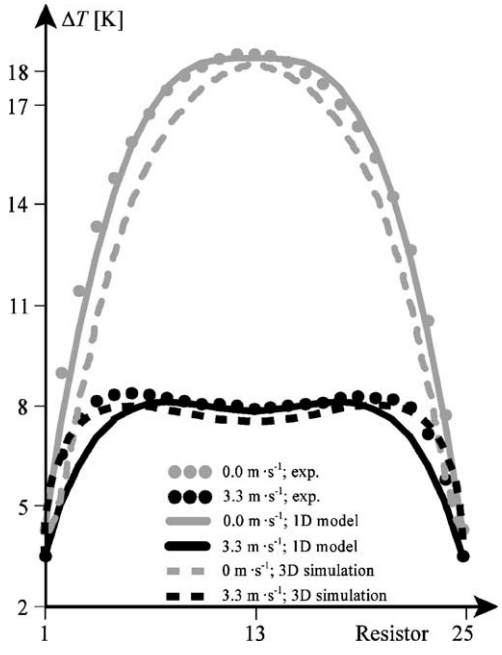

Fig. 13. Temperature difference of each resistor for a current of 2.5 mA (experimental/1D model/3D simulation for N_2).

We see that the values of the temperature difference ΔT we get from the 3D simulations are generally smaller than the corresponding experimental data, but the general shape of the curves corresponding to the 3D simulations are more similar to the experimental data than the shape of the curves obtained by the 1D model.

Also, we calculate the absolute values of the relative errors between the data offered by the 3D simulations and the experimental data for each resistor. On the other hand, we have calculated previously the absolute values of the relative errors between the data obtained by the 1D model simulation and the experimental data for each resistor. From these calculations, one concludes that the results from the 1D model as well as from the 3D simulations deviate by about 6% from the experimental data.

6. Conclusions

We present an 1D model for the heat transfer in an actuator–sensor structure for the determination of fluid and flow characteristics. The heat transfer mechanisms implied in the structure's functionality are detailed. The model consists in a linear second-order differential equation with variable coefficients associated with Dirichlet boundary conditions. This equation is solved straightforward using a standard finite difference method.

We compare the results derived by this 1D model with experimental data and also with the results from full 3D simulations of the fluid flow and heat transfer in the structure. The agreement we obtained between these curves (for about 6% for the case discussed in Fig. 13) is encouraging to use the 1D model further on in the design of this structure.

The 1D model described by Eq. (25) displays also a compact relation between temperature difference, velocity, thermal conductivity and kinematic viscosity of the fluid and the electric direct current. Therefore, this model is going also to be used for the design and measurement purposes, because velocity, thermal conductivity and kinematic viscosity of the fluid are three characteristics of the fluid we like to estimate.

The 1D model developed in this work is an important tool for the design of this structure as well as for the measurement purposes because of its compact form. This model is suitable for structure optimization and also for the identification problems implied by the structure's functionality.

The results detailed herein might be directly used for various thermal based actuators and sensors for flow control and measurement both in micro and macro world.

Acknowledgements

This work is funded by the Dutch Technology Foundation (STW) under the project TEL66-4408: resistive sensor–actuator structures for the determination of fluid and flow parameters. The authors thank Dr. John van Baar (Laboratory for Transducers Science and Technology, University of Twente) for discussions.

References

[1] A.F.P. van Putten, S. Middelhoek, Integrated silicon anemometer, IEEE Electron. Lett. 10 (1974) 425–426.
[2] K. Petersen, J. Brown, High-precision, high-performance mass-flow sensor with integrated laminar flow in micro-channels, in: Proceedings of Transducers'85, 1985, pp. 361–363.
[3] N. Damean, P.P.L. Regtien, Measurement concepts—from classical transducers to new MEMS, Measurement 27 (2000) 159–178.
[4] J. van Baar, R.J. Wiegerink, G.J.M. Krijnen, T.S.J. Lammerink, M.C. Elwenspoek, Sensitive thermal flow sensor based on a micro-machined two-dimensional resistor array, in: Proceedings of the 11th International Conference on Solid-State Sensors and Actuators, Munich, Germany, 2001.
[5] J. van Baar, R.J. Wiegerink, G.J.M. Krijnen, T.S.J. Lammerink, M.C. Elwenspoek, Distributed flow sensor based on a micro-machined resistor array, Sens. Actuators A, submitted for publication.
[6] P. Gravesen, J. Branebjerg, O.S. Jensen, Microfluidics—a review, J. Micromech. Microeng. 3 (1993) 168–182.
[7] A. Nathan, H. Baltes, Microstructure CAD—Physical and Computational Aspects, Springer-Verlag, Wien, 1999.
[8] F.P. Incropera, D.P. DeWitt, Fundamentals of Heat and Mass Transfer, fourth ed., Wiley, New York, 1996.
[9] N. Damean, P.P.L. Regtien, Velocity field of the fully developed laminar flow in a hexagonal duct, Sens. Actuators A 92 (2001) 144–151.
[10] N. Damean, P.P.L. Regtien, Poiseuille number for the fully developed laminar flow through hexagonal ducts etched in ⟨1 0 0⟩ silicon, Sens. Actuators A 90 (2001) 96–101.
[11] M. Ashauer, H. Glosch, F. Hedrich, N. Hey, H. Sandmaier, W. Lang, Thermal flow sensor for liquids and gases based on combinations of two principles, Sens. Actuators A 73 (1999) 7–13.
[12] U. Dillner, E. Kessler, S. Poser, V. Baier, J.V. Müller, Thermal simulation of a micromachined thermopile-based thin-film gas flow sensor, Microelectron. J. 29 (1998) 291–297.
[13] K. Chen, T.-E. Wu, Thermal analysis and simulation of the micro channel flow in miniature thermal conductivity detectors, Sens. Actuators A 79 (2000) 211–218.
[14] A.I.K. Lao, T.M.H. Lee, I.M. Hsing, N.Y. Ip, Precise temperature control of microfluidic chamber for gas and liquid phase reactions, Sens. Actuators A 84 (2000) 11–17.
[15] W.M. Rohsenow, J.P. Harnett, Y.I. Cho, Handbook of Heat Transfer, third ed., McGraw-Hill, New York, 1998 (Chapter 6).
[16] A.J. Chapman, Heat Transfer, Macmillan, New York, 1984.
[17] A. Bejan, Heat Transfer, Wiley, New York, 1993.
[18] M.M. Yovanovich, Dimensionless shape factors and diffusion lengths of three-dimensional bodies, in: Proceedings of the ASME/JSME Thermal Engineering Conference, vol. 1, 1985, pp. 103–114.
[19] F.L.A. Ganzevles, C.W.M. van der Geld, The shape factor of conduction in a multiple channel slab and the effect of non-uniform temperatures, Int. J. Heat Mass Transfer 40 (1997) 2493–2498.
[20] V.B. Svetovoy, I.A. Winter, Model of the μ-flown microphone, Sens. Actuators A 86 (2000) 171–181.
[21] T.S. Chen, B.F. Armaly, N. Ramachandran, Correlations for laminar mixed convection flows on vertical, inclined and horizontal flat plates, J. Heat Transfer 108 (1986) 835–840.
[22] F.M. White, Viscous Fluid Flow, second ed., McGraw-Hill, New York, 1991.
[23] O. Paul, H. Baltes, Determination of thermophysical properties of CMOS IC polysilicon, Sens. Actuators A 41 (1994) 161–164.
[24] B.W. van Oudheusden, Silicon thermal sensors, Sens. Actuators A 30 (1992) 5–26.

[25] B.W. van Oudheusden, The thermal modelling of a flow sensor based on differential convective heat transfer, Sens. Actuators A 29 (1991) 93–106.
[26] M.A. Lévêque, Les lois de la transmission de chaleur par convection, Ann. Mines 13 (1928) 201–239.
[27] L.V. King, On the convection of heat from small cylinders in a stream of fluid: determination of the convection constants of small platinum wires with applications to hot-wire anemometry, Phil. Trans. R. Soc. Lond. A 214 (1914) 373–432.
[28] Y.-C. Tai, R.S. Müller, Lightly doped polysilicon bridge as an anemometer, in: Proc. of Transducers 87 (1987) 360–363.
[29] A.F.P. van Putten, J.A.M. van Putten, M.J.A.M. van Putten, Silicon thermal anemometry: developments and applications, Meas. Sci. Technol. 7 (1996) 1360–1377.
[30] S.J. Kim, S.P. Jang, Experimental and numerical analysis of heat transfer phenomena in a sensor tube of a mass flow controller, Int. J. Heat Mass Transfer 44 (2001) 1711–1724.
[31] N.R. Swart, A. Nathan, Flow-rate microsensor modelling and optimisation using SPICE, Sens. Actuators A 34 (1992) 109–122.
[32] CFD Research Corporation, CFD-ACE+ software package, 215 Wynn Drive, Huntsville, AL 35805, USA.

Biographies

Nicolae Damean received the MSc and PhD (magna cum laude) degrees in electrical engineering from the Technical University of Iaşi, Romania, the MSc degree in mathematics from the University of Iaşi, Romania, and the PhD degree in engineering from the University of Twente, The Netherlands, in 1987, 1999, 1993 and 2002, respectively. From 1987 to 1990, he was with the Transducers and Self-Controllers Factory, Romania. From 1990 to 1997, he was successively an assistant professor and a lecturer at the Department of Electrical Engineering, Laboratory for Measurements and Materials, Technical University of Iaşi, Romania. From 1998 to 2002, he was a research assistant at the Department of Electrical Engineering, Laboratory for Measurement and Instrumentation, University of Twente, The Netherlands. Since 2002, he has been a postdoctoral fellow at the Department of Chemistry and Chemical Biology, Harvard University, USA. His current research interests are measurement science, micro- and nano-technology.

Paul P.L. Regtien received the MSc and PhD degrees from the Delft University of Technology, The Netherlands in 1970 and 1981, respectively. From 1970, he has been with the Department of Electrical Engineering of that University. From 1981 to 1982, he was with Endress und Hauser, Germany, where he worked on high temperature humidity measurement systems. Since 1994, he is a full professor at the Department of Electrical Engineering, University of Twente, The Netherlands, and head of the Laboratory for Measurement and Instrumentation. Present research activities are imaging (optical, acoustic, tactile), computer vision, mechatronics, sensor technology and instrumentation.

Miko Elwenspoek was born in Eutin, Germany, in 1948. He studied physics at the Free University of Berlin, Berlin, Germany, and received the PhD degree from the Free University of Berlin in 1983. His PhD research involved relaxation measurements on liquid metals and alloys, in particular alkali metal alloys. From 1977 to 1979, he studied lipid double layers. In 1983, he moved to the University of Nijmegen, Nijmegen, The Netherlands, to study crystal growth of organic crystals. In 1987, he joined the University of Twente, Enschede, The Netherlands, to take charge of the Laboratory for Transducers Science and Technology, MESA+ Research Institute. He has been a professor since 1996. His research include micro-electro-mechanical systems, fabrication techniques such as the physical chemistry of wet chemical anisotropic etching, reactive ion etching, wafer bonding, chemical–mechanical polishing, and the materials science of various thin films.